Active control of multi-input hydraulic journal bearing system

Jen-Chen Chuang[1], Chi-Yin Chen[2], Jia-Ying Tu[*]

Advanced Control and Dynamic Test Laboratory (ACDTLab), Department of Power Mechanical Engineering, National Tsing Hua University, Hsinchu 300, Taiwan

E-mail: jytu@pme.nthu.edu.tw

Abstract. Because of the advantages of high accuracy, high capacity, and low friction, the development of hydrostatic bearing for machine tool receives significant attention in the last decades. The mechanics and mechanical design of hydrostatic journal bearing with capillary restrictors has been discussed in literature. However, pragmatically, the undesired loading effects of cutting force tend to result in resonance and instability of the rotor and damage the shaft during operation. Therefore, multi-input, active flow control using state feedback design is proposed in this paper. To this purpose, the proportional pressure valves are added to the hydraulic system as active control devices, and the linearised models of the bearing and valve are discussed and identified. Simulation and experimental work is conducted to verify the proposed active control and parameter identification techniques. The results show that the unbalance responses of the rotor are reduced by the proposed state feedback controller, which is able to regulate the flow pressure effectively, thus enhancing the stability and accuracy of the hydraulic journal bearing.

1. Introduction

With the development of manufacturing technology, the demand for high-precision machine tools increases all over the world. Hydrostatic bearings are widely used in large rotating machine because of its advantages of low friction, high stiffness, high precision, and long sustainability. This paper considers the hydrostatic bearing which constitutes the lubricant plain bearing, that generates dynamic pressure to support its journal. In between the journal and the bearing, the gap is filled with high-pressure oil film, which is input through the restrictors to the recesses. The characteristics of the oil film, such as the thickness and stiffness, dominate the accuracy and stability of the journal bearing system. The film thickness is influenced by the applied load, supply pressure, and the restrictor resistance. Therefore, pressure compensation for maintaining the oil film thickness becomes an important issue.

Currently, many pressure control/compensation devices are used in the hydrostatic power system and the bearing mechanism, in order to sustain the oil film thickness and stiffness. Such devices include capillary restrictors, membrane-type restrictors, and servo valves. For example, in the presence of unwanted external load, Slocum, Scagnetti, Kane, and Brunner studied self-adjusting structure design to regulate the hydraulic pressure and balance the bearing system [1]. Lewis used theoretical and experimental approaches to study different types of pressure regulating mechanism, in order to

investigate the changes of oil film stiffness [2]. However, the capillary restrictor and membrane-type restrictors are passive pressure regulation devices, which may not be able to adjust the flow pressure actively and promptly in real-time. Because the mechanical design could not improve the performance of hydrostatic bearing further, active pressure regulating techniques are discussed in literature. For example, reference [3] established an active control technology with servo valves to adjust the oil film thickness; however, the cost would be very high.

This paper preliminarily develops a multi-input control method via state feedback design, in order to adjust the input pressure and oil film thickness of hydraulic bearing. The control method is meant to be realized using proportional pressure valves, which would be cheaper and more practical than servo valves. Section 2 presents the mathematical model of the multi-input hydraulic journal bearing system. The state feedback control algorithm is used for pressure compensation, as discussed in Section 3. Section 4 shows the simulation results of the multi-input control of hydraulic journal bearing system using MATLAB/Simulink. In addition, the experimental apparatus and the system identification results, which include the major control device of a proportional pressure valve, are presented in Section 4. Finally, a conclusion is drawn.

Table 1. Notations and parameters for hydrostatic bearing.

Symbol	Description	Value
A_e	effective bearing area	1600 (mm^2)
$\mathbf{F}_d$	measureable disturbance input matrix	N/A
K	feedback gain matrix	N/A
K_{ij}	bearing stiffness coefficient	N/A
m	mass of shaft	300 (kg)
P_s	supply pressure	30 (bar)
W	external load	100 (N)
β	pressure ratio	0.5
C_{ij}	bearing damping coefficient	N/A
δ_x	displacement along the x axis	N/A
δ_y	displacement along the y axis	N/A
θ	angle between W and the x axis	35°

2. Development of the mathematical model

This section introduces the control loop of the hydraulic bearing system first, and then explores the mathematical model of the bearing mechanism. **Figure 1** shows the proposed control scheme of the hydrostatic journal bearing system, which is constituted of the major components of hydraulic power system, restrictor, proportional pressure valve, bearing, real-time control system, and sensors. The proportional pressure valve is a part of the controlled plant for adjusting the input pressure of the restrictor. The rotor is equipped with an encoder in order to measure the rotational position. In addition, pressure sensors are installed in the loop for monitoring the pressure variations. All the measured signals are fed back to the real-time control system, which computes the required control signal to adjust the orifice of the proportional pressure valve.

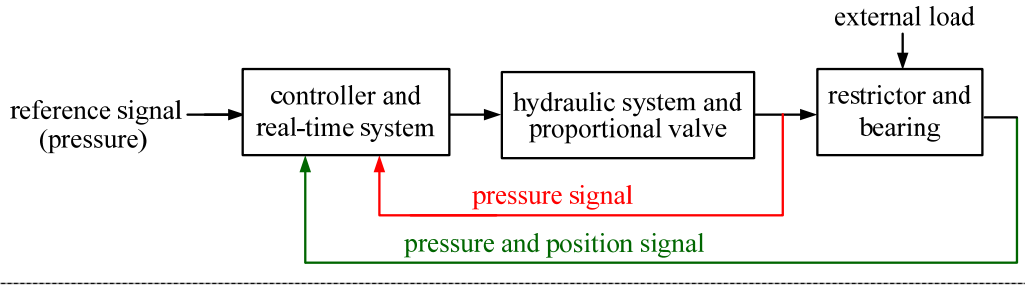

Figure 1. Control loop of the hydraulic journal bearing system.

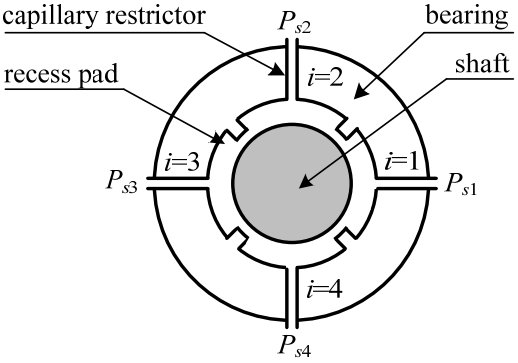

Figure 2. The cross-section scheme of the journal bearing system.

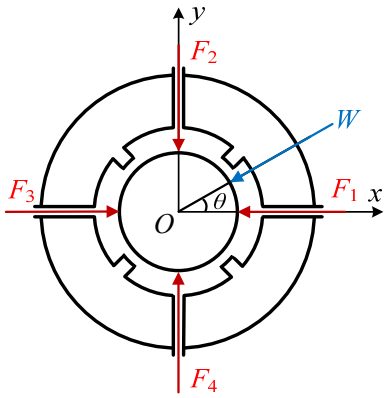

Figure 3. The free body diagram of the hydrostatic bearing.

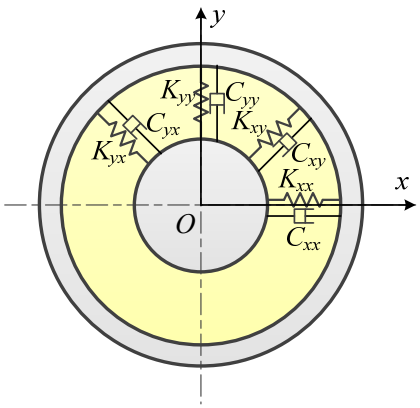

Figure 4. The damping and stiffness coefficients of oil film.

Furthermore, the mathematical model of the bearing is discussed. The cross-section scheme of the journal bearing system is shown in **Figure 2**, which includes four restrictors and recess pads. Each recess is equipped with its own capillary restrictor so that the bearing has certain self-aligning capability, called passive compensation. In the centre of the bearing, a shaft is installed, which is rotated by an electric motor. Therefore, high-pressure oil is imported through the restrictors and recesses to generate the high-stiffness oil film, which maintains the smooth, fast, and continuous rotation of the shaft. Assuming that the flow of each restrictor is equal without external load applied, the four recesses provide the same forces, F_1, F_2, F_3, and F_4, to balance the shaft. When the hydrostatic journal bearing is applied by an external load, W, the free body diagram of the hydrostatic bearing is

shown in **Figure 3**. The angle between the force direction and the x axis is denoted as θ. As W is applied, the centre position of the shaft is offset from the origin O, and thus the control objective is to reduce the eccentricity and push the shaft back to the origin.

According to the Newton's second law and **Figure 3**, the dynamic characteristics of the oil film can be modelled via linearised damping and stiffness coefficients [4]. Therefore, the equations of motion of the shaft with the external load are written as:

$$\begin{aligned} m\ddot{\delta}_x + C_{xx}\dot{\delta}_x + C_{xy}\dot{\delta}_y + K_{xx}\delta_x + K_{xy}\delta_y &= -F_1 + F_3 - W\cos\theta \\ m\ddot{\delta}_y + C_{yx}\dot{\delta}_x + C_{yy}\dot{\delta}_y + K_{yx}\delta_x + K_{yy}\delta_y &= -F_2 + F_4 - W\sin\theta \end{aligned} \tag{1}$$

where m is the mass of the shaft, and δ_x and δ_y are the displacements of the shaft centre along the x and y axes, respectively. The linearised damping coefficients of the oil film are denoted as C_{xx}, C_{xy}, C_{yx}, and C_{yy}; in addition, K_{xx}, K_{xy}, K_{yx}, and K_{yy} are the linearised stiffness coefficients. The scheme of the coefficients and the dynamic model is shown in **Figure 4**, where the yellow part represents the oil film and the grey parts are the shaft and bearing. According to [4], the pressure multiplied by the area is equal to the force, and thus, the applied forces as a result of the recess pressure are expressed as $F_1 = \beta A_e P_{s1}$, $F_2 = \beta A_e P_{s2}$, $F_3 = \beta A_e P_{s3}$, and $F_4 = \beta A_e P_{s4}$, where β is the ratio between the input and output pressure of the recess, A_e is the effective bearing area, and P_{s1}, P_{s2}, P_{s3}, and P_{s4} are the input pressure of recess pads. Substituting these force expressions into Equation (1), the equations of motion are arranged to:

$$\begin{aligned} \ddot{\delta}_x &= -\frac{C_{xx}}{m}\dot{\delta}_x - \frac{C_{xy}}{m}\dot{\delta}_y - \frac{K_{xx}}{m}\delta_x - \frac{K_{xy}}{m}\delta_y - \frac{\beta A_e}{m}P_{s1} + \frac{\beta A_e}{m}P_{s3} - \frac{\cos\theta}{m}W \\ \ddot{\delta}_y &= -\frac{C_{yx}}{m}\dot{\delta}_x - \frac{C_{yy}}{m}\dot{\delta}_y - \frac{K_{yx}}{m}\delta_x - \frac{K_{yy}}{m}\delta_y - \frac{\beta A_e}{m}P_{s2} + \frac{\beta A_e}{m}P_{s4} - \frac{\sin\theta}{m}W \end{aligned} \tag{2}$$

Equation (2) linearizes and represents the equations of motion of the shaft, and is used for the state feedback control design in next section.

3. Development of the control algorithm

The linearised mathematical model of the hydrostatic bearing system has been established in the previous section. In this section, the state feedback control (SFC) algorithm is used to compensate for the flow pressure and thus control the position of the shaft centre. This requires transform Equation (2) into a state-space model, and the scheme of the SFC block diagram is shown in **Figure 5**. Here, Equation (2) is the plant to be controlled. Assuming that the input pressures of the four recesses are the input control signals, which are defined as $u_1 = P_{s1}$, $u_2 = P_{s2}$, $u_3 = P_{s3}$, and $u_4 = P_{s4}$, Equation (2) needs to be modified to:

$$\begin{aligned} \ddot{\delta}_x &= -\frac{C_{xx}}{m}\dot{\delta}_x - \frac{C_{xy}}{m}\dot{\delta}_y - \frac{K_{xx}}{m}\delta_x - \frac{K_{xy}}{m}\delta_y - \frac{\beta A_e}{m}u_1 + \frac{\beta A_e}{m}u_3 - \frac{\cos\theta}{m}W \\ \ddot{\delta}_y &= -\frac{C_{yx}}{m}\dot{\delta}_x - \frac{C_{yy}}{m}\dot{\delta}_y - \frac{K_{yx}}{m}\delta_x - \frac{K_{yy}}{m}\delta_y - \frac{\beta A_e}{m}u_2 + \frac{\beta A_e}{m}u_4 - \frac{\sin\theta}{m}W \end{aligned} \tag{3}$$

Then the state variables are selected as $x_1 = \delta_x$, $x_2 = \dot{x}_1$, $x_3 = \delta_y$, and $x_4 = \dot{x}_3$. With the four state variables, Equation (3) is transformed into a set of first-order state-space equation as follows:

$$\begin{aligned}
\dot{x}_1 &= x_2 \\
\dot{x}_2 &= -\frac{C_{xx}}{m}x_2 - \frac{C_{xy}}{m}x_4 - \frac{K_{xx}}{m}x_1 - \frac{K_{xy}}{m}x_3 - \frac{\beta A_e}{m}u_1 + \frac{\beta A_e}{m}u_3 - \frac{\cos\theta}{m}W \\
\dot{x}_3 &= x_4 \\
\dot{x}_4 &= -\frac{C_{yx}}{m}x_2 - \frac{C_{yy}}{m}x_4 - \frac{K_{yx}}{m}x_1 - \frac{K_{yy}}{m}x_3 - \frac{\beta A_e}{m}u_2 + \frac{\beta A_e}{m}u_4 - \frac{\sin\theta}{m}W
\end{aligned} \tag{4}$$

In addition, the controlled outputs are defined as $\mathbf{y} = [\delta_x \quad \delta_y]^T = [x_1 \quad x_3]^T$, and thus the entire state-space system is given by:

$$\begin{aligned}
\underbrace{\begin{bmatrix} \dot{x}_1 \\ \dot{x}_2 \\ \dot{x}_3 \\ \dot{x}_4 \end{bmatrix}}_{\dot{\mathbf{x}}} &= \underbrace{\begin{bmatrix} 0 & 1 & 0 & 0 \\ -\frac{K_{xx}}{m} & -\frac{C_{xx}}{m} & -\frac{K_{xy}}{m} & -\frac{C_{xy}}{m} \\ 0 & 0 & 0 & 1 \\ -\frac{K_{yx}}{m} & -\frac{C_{yx}}{m} & -\frac{K_{yy}}{m} & -\frac{C_{yy}}{m} \end{bmatrix}}_{\mathbf{A}} \underbrace{\begin{bmatrix} x_1 \\ x_2 \\ x_3 \\ x_4 \end{bmatrix}}_{\mathbf{x}} \\
&+ \underbrace{\begin{bmatrix} 0 & 0 & 0 & 0 \\ -\frac{\beta A_e}{m} & 0 & \frac{\beta A_e}{m} & 0 \\ 0 & 0 & 0 & 0 \\ 0 & -\frac{\beta A_e}{m} & 0 & \frac{\beta A_e}{m} \end{bmatrix}}_{\mathbf{B}} \underbrace{\begin{bmatrix} u_1 \\ u_2 \\ u_3 \\ u_4 \end{bmatrix}}_{\mathbf{u}} + \underbrace{\begin{bmatrix} 0 \\ -\frac{\cos\theta}{m}W \\ 0 \\ -\frac{\sin\theta}{m}W \end{bmatrix}}_{\mathbf{F}_d}
\end{aligned} \tag{5}$$

$$\mathbf{y} = \begin{bmatrix} x_1 \\ x_3 \end{bmatrix} = \underbrace{\begin{bmatrix} 1 & 0 & 0 & 0 \\ 0 & 0 & 1 & 0 \end{bmatrix}}_{\mathbf{C}} \mathbf{x} \tag{6}$$

Equations (5) and (6) are written in a concise form below:

$$\dot{\mathbf{x}} = \mathbf{A}\mathbf{x} + \mathbf{B}\mathbf{u} + \mathbf{F}_d \tag{7}$$

$$\mathbf{y} = \mathbf{C}\mathbf{x} \tag{8}$$

where **A**, **B**, and **C** are the plant, input, and output matrices, respectively, and $\mathbf{x} = [x_1 \ x_2 \ x_3 \ x_4]^T$ and $\mathbf{u} = [u_1 \ u_2 \ u_3 \ u_4]^T$ correspond to the state and input vectors. The measureable disturbance input matrix is denoted as $\mathbf{F}_d$. Here, the SFC design assumes that **x** is fully measurable within the control loop, and the control law is proposed as:

$$\mathbf{u} = -\mathbf{K}\mathbf{x} \tag{9}$$

where **K** is the feedback gain matrix. With the substitution of Equation (9) into (7), the overall closed-loop dynamics become:

$$\dot{\mathbf{x}} = \mathbf{A}\mathbf{x} + \mathbf{B}\left[-\mathbf{K}\mathbf{x}\right] = \left(\mathbf{A} - \mathbf{B}\mathbf{K}\right)\mathbf{x} \tag{10}$$

Stability is governed by the eigenvalues of (**A**−**BK**). Typically, to enhance the system performance, the location of the eigenvalue is selected to be faster than that of **A**. Control synthesis and simulation work are discussed in the next section.

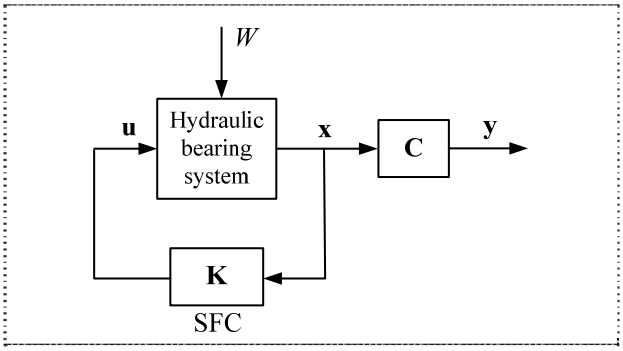

Figure 5. Design of state feedback controller.

4. Simulation and experiment results

In this section, the numerical simulation, data analysis, and experimental implementation are conducted using MATLAB/Simulink and dSPACE system; dSPACE provides an integration solution for the ADC/DAC hardware and MATLAB /Simulation software. The first part of this section discusses the SFC simulation work, followed by the implementation and identification results in the second part.

4.1. Simulation results

In Sections 2 and 3, the linearised model of the hydraulic bearing system and the design of SFC have been presented. Then, the control block diagram for pressure compensation is built in MATLAB /Simulink, as shown in **Figure 6**. Equations (5) and (6) are included in the pink block, and SFC is built in the green block. **Table 1** summarises the notations and parameter settings for simulation study. According to the plant model of Equation (5) and the parameters of **Table 1**, the open-loop poles are known at s = -3443.5, -144.7, -2.1, and 0.3. A pole in the right-hand plane of the Laplace domain shows instability. Thus, in order to improve the stability and enhance the regulation performance, the new closed-loop poles are assigned to be at s = -84, -84.001, -84.002, and -84.003. Thus, the state-feedback gain matrix of Equation (9) is computed as follows:

$$\mathbf{K} = 10^8 \times \begin{bmatrix} -3.73 & 4.269 & 4.375 & 1.875 \\ 4.375 & 1.875 & -1.228 & 4.269 \\ 3.73 & +4.269 & -4.375 & -1.875 \\ -4.375 & -1.875 & 12.28 & -4.269 \end{bmatrix} \tag{11}$$

The high gain reflects the required high-stiffness characteristics of the oil film.

In the simulation work, the cutting force, W, is modelled by a step function with the magnitude of 100 N lasting for 0.5 second, as shown in **Figure 7**a. The control performance is shown in **Figure 7**b, which displays the trajectories of the shaft centre; the blue-dotted and green-solid curves correspond to δ_x and δ_y. Although the external force offset the position of the shaft centre, SFC regulated the input pressure of the four recesses and pushed the shaft back to the central position in 0.1 s. **Figure 7** thus briefly verifies the proposed modelling and control techniques. In pragmatic work, the settling time would be required to be shorter than 0.1 s in order to achieve high-precision manufacturing of machine tool, and the external force would be much larger. Thus, the control gain tuning in relation to the machine tool performance will be discussed further in future work. In addition, the control signal for adjusting the input pressure is meant to be realised via proportional pressure valves, which is introduced in the subsequent section.

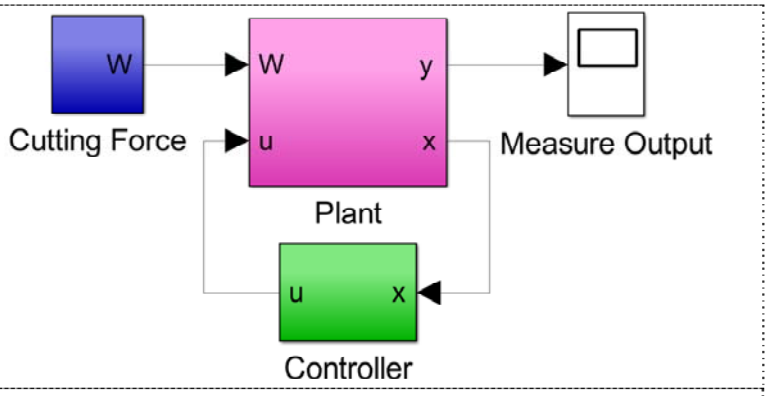

Figure 6. Simulink block diagram for the simulation of pressure compensation.

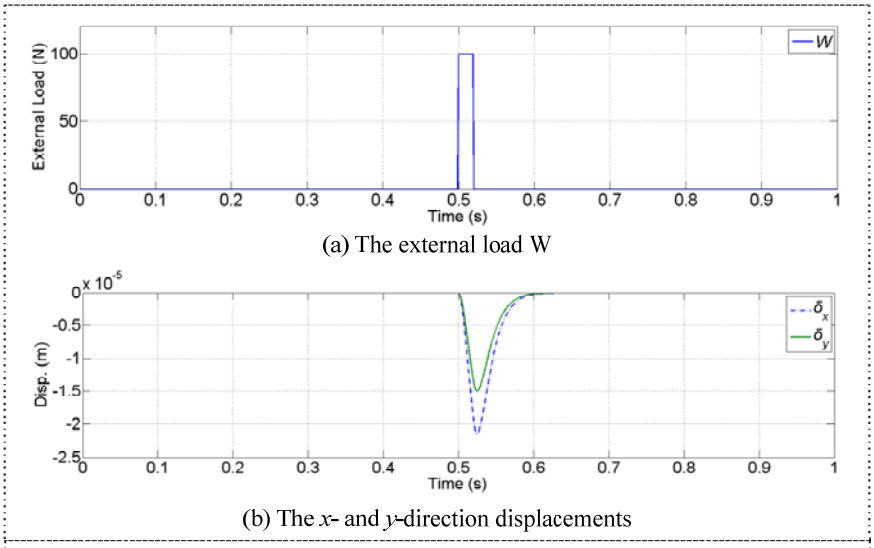

(a) The external load W

(b) The *x*- and *y*-direction displacements

Figure 7. The simulation results of pressure compensation using state feedback control: (a) the external load *W*, and (b) the *x*- and *y*-direction displacements.

4.2. Experimental work of system identification

For the purpose of realising the control scheme of Section 3, additional control devices must be installed in the hydraulic power system, beforehand the capillary restrictors. In this work, proportional pressure valves are utilised to adjust the input pressure of recesses. Here, only one proportional pressure valve is considered in the initial stage of experimental verification.

Figure 8 shows the circuit of the hydraulic system, including the major components of a proportional pressure valve, a pump, an oil tank, a filter, an accumulator, three pressure sensors, a proportional relief valve, input/output pipes, etc. **Figure 8** is realised in **Figure 9** for implementation study of pressure compensation. The pump, with a maximum flow of 14 L/min and maximum pressure of 50 bar, is used to supply the lubrication oil to the bearing system. The output pressure of the pump is adjustable by the relief valve. The proportional pressure valve is meant to be controlled to adjust the input pressure of the capillary restrictors. Three pressure sensors are connected to the input of the relief valve, the input of pressure valve, and the output of the hydraulic system, for the purpose of monitoring the pressure variations. Furthermore, the dSPACE system acts as a communication

interface between the software and hardware. The pressure sensor signal is read by ADC and the control command is sent to the proportional pressure valve via DAC, as illustrated in **Figure 10**.

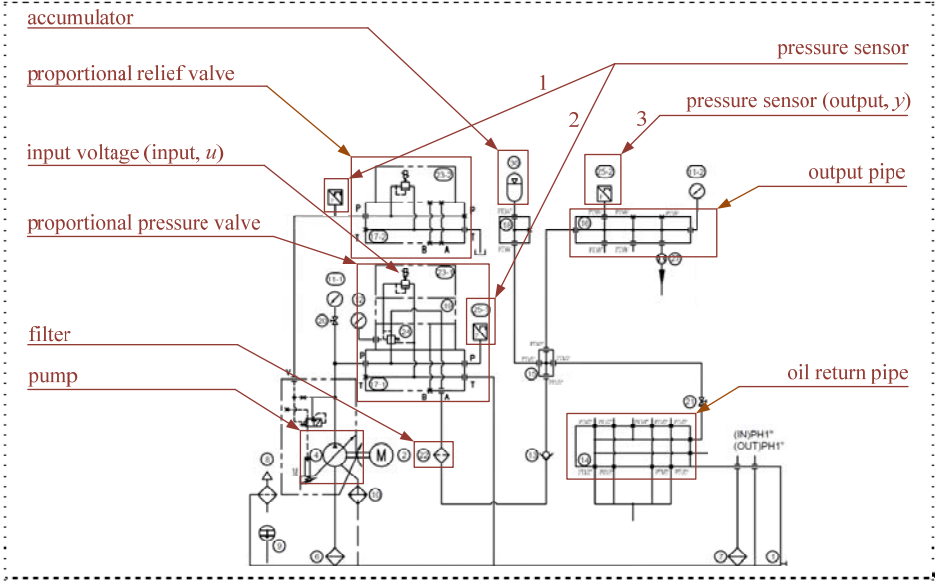

Figure 8. The circuit of the hydraulic power system.

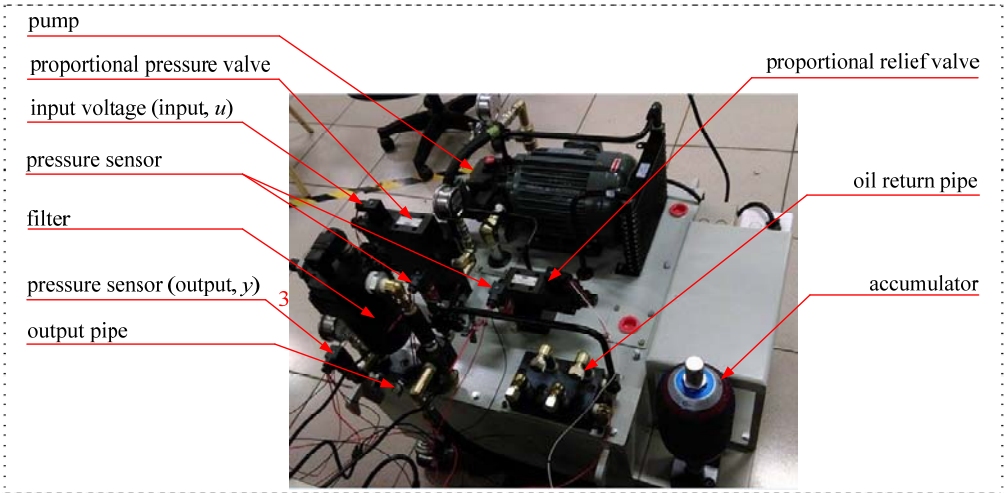

Figure 9. The equipment of hydraulic power system.

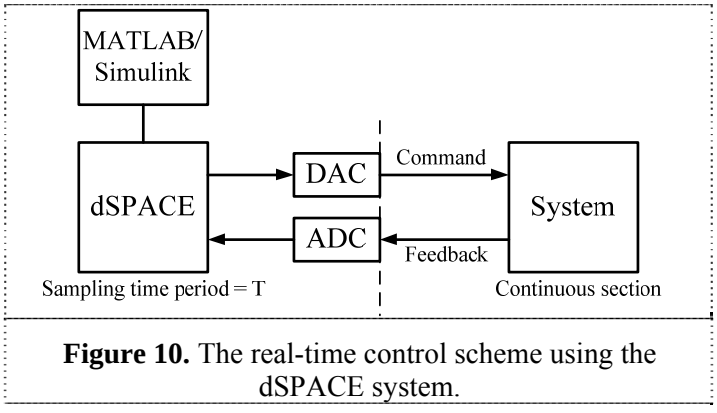

Figure 10. The real-time control scheme using the dSPACE system.

In the stage of dynamics analysis and control design, the linearised model of hydraulic power system can be obtained via the system identification techniques. In this identification work, a voltage input signal in sinusoidal form with a frequency of 0.25 Hz and an amplitude of 1 V was sent to the proportional pressure valve, and the output pressure of the hydraulic system was recorded. **Figure 8** indicates the location of the measured signals, and the output pressure of the hydraulic system is measured by the third pressure sensor. The data sampling interval was set to be 0.001 s. As shown in **Figure 11**, the green and red curves show the input voltage (u) of the proportional pressure valve in volt and the output pressure (y) of the hydraulic system in bar, respectively. The output signal, y, is equivalent to the input pressure of the restrictor, i.e. P_{s1}, P_{s2}, P_{s3}, or P_{s4}. From the input and output data, the combined nominal model of the proportional pressure valve, filter, and accumulator, was obtained via the *oe* function as follows:

$$G = \frac{y(s)}{u(s)} = \frac{3300.9s + 5609.6}{s^2 + 943.8s + 1132.7} \tag{12}$$

Equation (12) shows a second order model, and the low-frequency gain, damping ratio, and resonate frequency are 4.95 dB, 1.0 N·s/m, and 150 Hz, respectively. In addition, the simulated response based on Equation (12) was compared with the experimental data in **Figure 11**. The blue and red curves correspond to the experimental and simulated responses; the two curves almost matched, thus showing accurate identification work. In Equation (12), the relatively large low-frequency gain is as a result of unit difference, where the input and output units are in volt and bar, respectively. This issue can be improved via the scaling technique in future work. System identification using swept sinusoids with a range of frequencies will be carried out, in order to take the frequency-dependent dynamics into account. The obtained model will be combined with SFC to design the multi-input controller for the hydraulic power system.

5. Conclusions

This paper aims to develop the multi-input, active flow control method via state feedback for hydrostatic journal bearing system. The proportional pressure valves are added to the hydraulic system as the active control devices to modulate the input pressure to the restrictor. A linearised mathematical model of the hydraulic bearing system is developed in state-space form. The input pressure of the capillary restrictor is taken as the command signal, and the proportional pressure valve functions like an active control device. State feedback controller is designed to regulate the recess pressure; the results are verified via simulation work. Simulation results show that the proposed state feedback controller is able to regulate the input pressure and thus balance the response of the rotor. Experimental work of system identification is conducted to identify the transformed model of the proportional pressure valve. In future wok, the entire mathematical model of the hydraulic journal bearing system will be developed, which includes the bearing mechanism and the hydraulic power system. Meanwhile, the identified model of the proportional pressure valve will be transformed and integrated into the complete model. Then full pressure compensation technique, including the observer design, will be developed in order to enhance the performance of the control system.

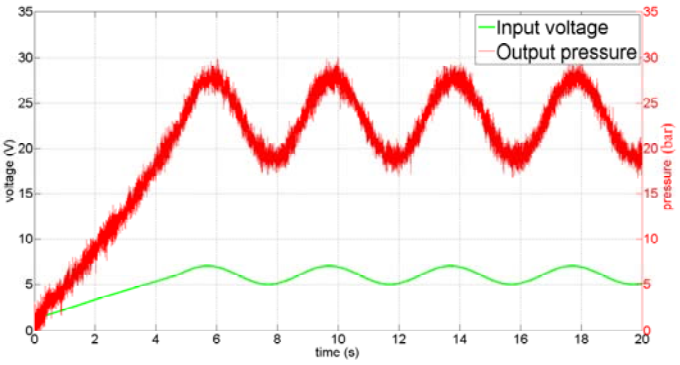

(a) The input voltage and output pressure signal

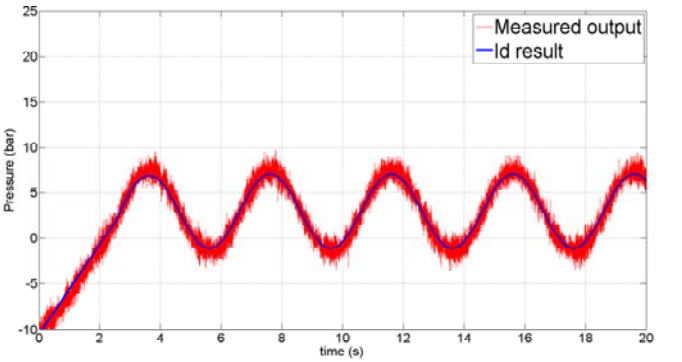

(b) The system identification result

Figure 11. The system identification result.

References

[1] Slocum A H *et al* 1995 *Design of self-compensated, water-hydrostatic bearings* vol 17 (Amsterdam: Elsevier) pp 173-185

[2] Lewis G K 1984 *The stiffness and static stability of compensated hydrostatic cylindrical-pad bearings* vol 198 (Suffolk: Mechanical) pp 285-292

[3] Shih M C and Shie J S 2013 *Recess Design and Dynamic Control of an Active Compensating Hydrostatic Bearing* vol 7 (Tokyo: J-Stage) pp 706-721

[4] Rowe W B 2012 *Hydrostatic, Aerostatic, and Hybrid Bearing Design* (Amsterdam: Elsevier)